

Effect of thermal annealing for W/ β -Ga₂O₃ Schottky diodes up to 600 °C

Minghan Xian, Chaker Fares, Fan Ren, Brent P. Gila, Yen-Ting Chen, Yu-Te Liao, Marko Tadjer, and Stephen J. Pearton

Citation: *Journal of Vacuum Science & Technology B* **37**, 061201 (2019); doi: 10.1116/1.5125006

View online: <https://doi.org/10.1116/1.5125006>

View Table of Contents: <https://avs.scitation.org/toc/jvb/37/6>


Published by the [American Vacuum Society](#)



Contact Hiden Analytical for further details:
W www.HidenAnalytical.com
E info@hiden.co.uk

CLICK TO VIEW our product catalogue

Instruments for Advanced Science



Gas Analysis

- dynamic measurement of reaction gas streams
- catalysis and thermal analysis
- molecular beam studies
- dissolved species probes
- fermentation, environmental and ecological studies



Surface Science

- UHV-TPD
- SIMS
- end point detection in ion beam etch
- elemental imaging - surface mapping



Plasma Diagnostics

- plasma source characterization
- etch and deposition process reaction kinetic studies
- analysis of neutral and radical species



Vacuum Analysis

- partial pressure measurement and control of process gases
- reactive sputter process control
- vacuum diagnostics
- vacuum coating process monitoring



Effect of thermal annealing for W/ β -Ga₂O₃ Schottky diodes up to 600 °C

Minghan Xian,¹ Chaker Fares,¹ Fan Ren,¹ Brent P. Gila,^{2,3} Yen-Ting Chen,⁴ Yu-Te Liao,⁴ Marko Tadjer,⁵ and Stephen J. Pearton^{3,a)}

¹Department of Chemical Engineering, University of Florida, Gainesville, Florida 32611

²Nanoscale Research Facility, University of Florida, Gainesville, Florida 32611

³Department of Materials Science and Engineering, University of Florida, Gainesville, Florida 32611

⁴Department of Electrical and Computer Engineering, National Chiao Tung University, Hsinchu 30010, Taiwan

⁵US Naval Research Laboratories, Washington, DC 20375

(Received 19 August 2019; accepted 12 September 2019; published 30 September 2019)

The electrical and structural properties of sputter-deposited W Schottky contacts with Au overlayers on n-type Ga₂O₃ are found to be basically stable up to 500 °C. The reverse leakage in diode structures increases markedly (factor of 2) for higher temperature annealing of 550–600 °C. The sputter deposition process introduces near-surface damage that reduces the Schottky barrier height in the as-deposited state (0.71 eV), but this increases to 0.81 eV after a 60 s anneal at 500 °C. This is significantly lower than conventional Ni/Au (1.07 eV), but W is much more thermally stable, as evidenced by Auger electron spectroscopy of the contact and interfacial region and the minimal change in contact morphology. The contacts are used to demonstrate 1.2 A switching of forward current to –300 V reverse bias with a reverse recovery time of 100 ns and a dI/dt value of 2.14 A/ μ s. The on/off current ratios were $\geq 10^6$ at –100 V reverse bias, and the power figure-of-merit was 14.4 MW cm^{–2}. Published by the AVS. <https://doi.org/10.1116/1.5125006>

I. INTRODUCTION

β -Ga₂O₃ is an ultrawide bandgap semiconductor with attractive potential for power switching applications beyond the performance of SiC or GaN.^{1–9} In particular, an early adoption possibility is in rectifiers as part of hybrid power inverter units that also include Si thyristors or insulated gate bipolar transistors.^{10–15} Economic analyses have suggested that such Ga₂O₃ devices could deliver SiC-like performance at Si-like cost.^{16,17} There have been impressive demonstrations of vertical and lateral geometry Ga₂O₃ rectifiers, with breakdown voltages above 2 kV, total forward currents >30 A, and switching of currents up to 0.7 A.^{18–23} The important aspects of these devices that need development are the thermal management structures as well as the stability of the contacts and field management approaches.^{8,13,24} The usual top-side Schottky metal is Ni/Au, which has a decent barrier height (>1 eV), but limited thermal stability. Since power rectifiers will need to operate at elevated temperatures even with optimized thermal management designs,²⁵ the stability of the rectifying contact is crucial.^{26–32} There have been a number of reports of the use of W for Schottky contacts on Ga₂O₃. Yao *et al.*²⁸ investigated the thermal stability of W on β -Ga₂O₃ for annealing up to 800 °C. In a separate study,^{30,31} the same group examined the optimum surface treatments for W on Ga₂O₃ and concluded that surface states had a prominent effect on barrier properties.^{30,31} Fares *et al.*³² showed that W-based contacts are more thermally stable than conventional Ni-based Schottky contacts. There are, as yet, no studies of the high current switching characteristics.

It is clearly of interest to examine the thermal stability and high temperature contact properties of W on Ga₂O₃ in more

detail. The previous studies have established that the barrier height of W is lower than for Ni and other common metals, as expected from its work function, but it is still of interest for high temperature applications. In this paper, we report the thermal stability of W/Au Schottky electrodes and their applicability to power switching at Ampere levels, as well as on/off current ratios out to –100 V reverse bias. Tungsten is one of the most thermally stable metals, with a melting point of 3422 °C and showed excellent chemical stability to the Au overlayer as well as the underlying Ga₂O₃.

II. EXPERIMENT

The starting material was Sn-doped ($n = 3.6 \times 10^{18}$ cm^{–3}) β -Ga₂O₃ single crystal (001) substrates grown by the edge-defined film-fed technique, with a 10 μ m Si doped β -Ga₂O₃ epitaxial layer grown on top of this substrate. After growth, the epi surface was planarized by chemical mechanical polishing. The n-drift region was grown by halide vapor phase epitaxy with a carrier concentration of 3.5×10^{16} cm^{–3}, obtained from capacitance-voltage measurements. For electrical measurements in vertical geometry, full-area back Ohmic contact deposition of Ti/Au (20/80 nm) by electron-beam evaporation, followed by annealing at 550 °C in N₂ for 30 s, was used to form the Ohmic contacts.

The front side of the structures was cleaned with HCl and then treated in O₃ for 20 min to remove residual hydrocarbons and other surface species. It is known that residual contaminants like hydroxyl species may dominate the surface band-bending on β -Ga₂O₃.³³ A bilayer of 40 nm Al₂O₃ and 360 nm SiN_x was used as the field plate,²⁴ and dilute buffered oxide etch (BOE) was used to etch the dielectric opening. The samples were patterned again for W (or Ni) deposition. Then, 20 nm W was deposited by dc sputtering

^{a)}Electronic mail: spearl@mse.ufl.edu

using a 3-in. target of pure W. The dc power was 400 W, and the process pressure was 5 mTorr in pure Ar ambient. Following W deposition, a 340 nm layer of Au was deposited by e-beam evaporation to reduce the sheet resistance of the contact and prevent oxidation of the tungsten. Contact sizes ranged from 40 to 200 μ m diameter circles to 800 μ m squares. This was done to examine the effect of contact geometry and size on the normalized leakage current density. For comparison, standard Ni (20 nm)/Au (80 nm) Schottky contacts deposited by e-beam evaporation and patterned by lift-off were fabricated on the same epi structures. Both Ni/Au and W/Au devices are formed by using the standard lift-off process.

Current-voltage (I-V) characteristics were measured with an HP 4156 parameter analyzer in air at 25 °C. We defined reverse breakdown to be the voltage at which the reverse current density reaches 10 mA cm². Capacitance-voltage (C-V) measurements were taken with an Agilent 4284A Precision LCR Meter. The device on-off ratio was measured at a fixed forward current of 200 mA and 0 to -100 V for reverse current and was in the range of 10⁶-10⁸. The morphology of annealed samples was quantified through atomic force microscopy, while the depth profiles of each element in the contact stack were measured by Auger electron spectroscopy (AES) with concurrent Ar sputtering.

III. RESULTS AND DISCUSSION

Figure 1(a) shows a comparison of the room temperature current density (J)-voltage (V) characteristics from the W/Au and Ni/Au Schottky contacts on β -Ga₂O₃. The higher reverse leakage current and forward current for W/Au show this has a lower barrier height than for Ni/Au, as reported previously.^{28,30,32} The W/Au samples were annealed for different times at 500 °C and the Schottky barrier height, Φ_B , and ideality factor, n , extracted from the I-V characteristics in Fig. 1(b) by fitting the linear region of the I-V curves to the thermionic emission model.³⁴⁻³⁷ A compilation of these data is shown in Table I. The barrier height for W on (001) β -Ga₂O₃ is 0.71 eV in the as-deposited state, which will include lowering due to the presence of sputter damage. Yao *et al.*^{28,30} have reported that electron-beam evaporation yields higher quality (near unity ideality factor) Schottky diodes in comparison to sputter-deposited contacts. After a 60 s anneal at 500 °C to remove this surface damage, the barrier height is 0.81 eV. This compares to a value of 0.97 eV for W contacts on (-201) β -Ga₂O₃.³² The anisotropy of many material properties for Ga₂O₃ is well-established,³⁸ including thermal conductivity, dielectric constant, mobility, and lattice constants. There is only a weak correlation of barrier height to metal work function, which indicates that there is at most only a partial Fermi level pinning due to defects and/or surface states, particularly on the (201) surface for which most data have been reported.^{28,31,36} Behavior closer to that predicted by the Schottky-Mott model is observed for (010) orientation.^{28,30,31,36} It will be interesting to build up a database of barrier heights for the same metals on different orientations of Ga₂O₃ to establish

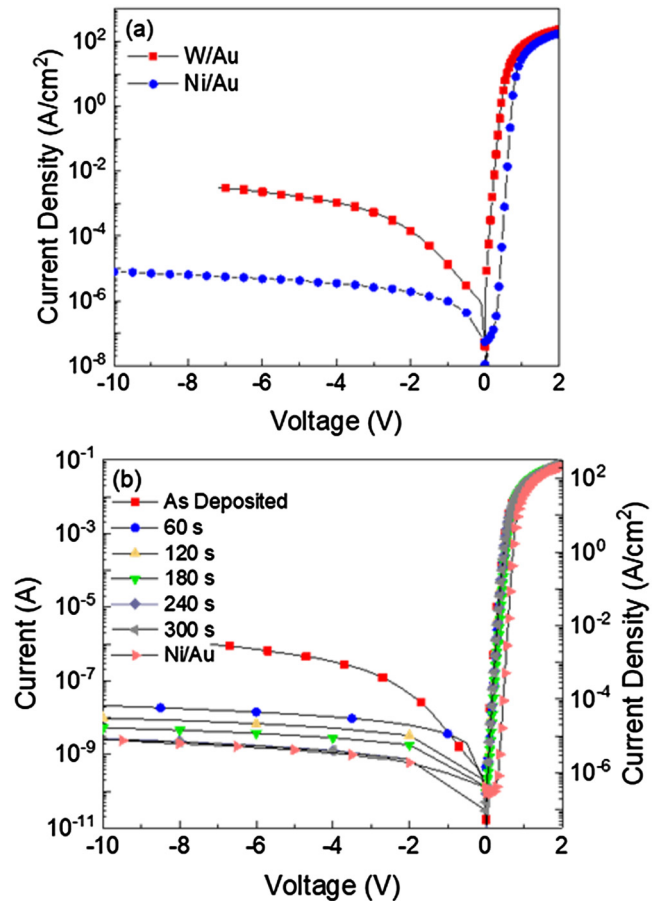


FIG. 1. Current density-voltage characteristics of 200 μ m diameter Ga₂O₃ based rectifiers fabricated with Ni/Au and W/Au as Schottky metal contact (a). Current density-voltage characteristics of 200 μ m diameter Ga₂O₃ Schottky with W/Au contact annealed at 500 °C for different annealing times (b).

the extent of the effect of crystal anisotropy.³⁹⁻⁴² Note in Table I that, within experimental error, the barrier height for W shows little change with annealing time at 500 °C.

Figure 2 shows the on/off ratio measured at a fixed forward bias of -1 V to a reverse voltage between 0 and -100 V. This is in the range of 10⁶-10⁸ over this bias voltage range, provided the sputtering damage is removed.

TABLE I. Schottky barrier height, ideality factor, and on-resistance of 200 μ m diameter Ga₂O₃ Schottky with W/Au contact annealed at 500 °C for different annealing times.

Annealing time at 500 °C	Schottky barrier height (± 0.03 eV)	Ideality factor (± 0.05)	On-resistance (m Ω cm ²)
As deposited	0.71	1.30	9.0
60 s	0.81	1.12	9.8
120 s	0.78	1.14	9.8
180 s	0.80	1.19	8.6
240 s	0.77	1.15	9.7
300 s	0.77	1.13	8.5
Ni/Au contact (as deposited)	1.07	1.02	10.5

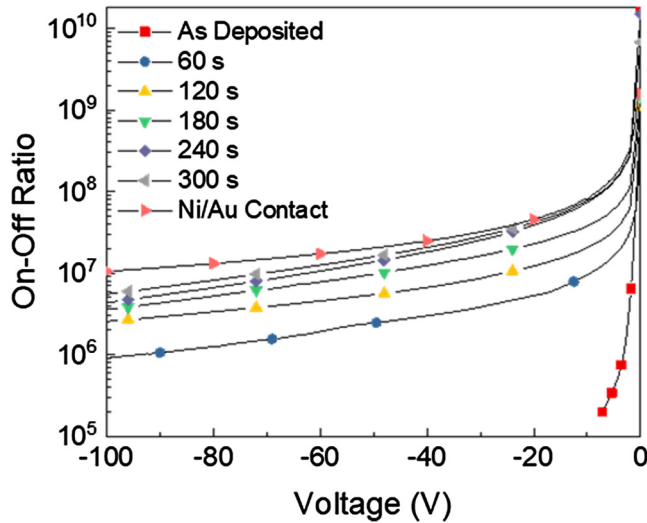


FIG. 2. Rectifier on-off ratio from 0 to -100 V for $200\text{ }\mu\text{m}$ diameter diodes annealed at $500\text{ }^{\circ}\text{C}$ with different annealing times.

Note that the as-deposited samples show a much degraded on/off ratio. The Ni/Au contact shows values that are comparable to the W/Au contacts annealed at $500\text{ }^{\circ}\text{C}$ for 300 s. This is a useful result in that it shows that even with the lower barrier height, the W-based contact under optimized conditions can achieve similar values of on/off ratio to Ni/Au, but with superior thermal stability.

Figure 3 shows the reverse breakdown characteristics for a group of W/Au diodes annealed at 500 , 550 , and $600\text{ }^{\circ}\text{C}$. The leakage current at -100 V basically doubles after annealing at $550\text{ }^{\circ}\text{C}$, showing that above $500\text{ }^{\circ}\text{C}$, the W contacts degrade. The breakdown voltages, defined as the voltage at which the reverse current density is 10 mA cm^{-2} , were ~ 350 V for the W contacts at this doping concentration of $3.5 \times 10^{16}\text{ cm}^{-3}$. These results produce a power figure-of-merit, V_B^2/R_{on} , of 14.4 MW cm^{-2} with the on-resistance reported in Table I.

Figure 4 (top) shows a consistent breakdown, independent of contact size for the circular contacts. Note that the square

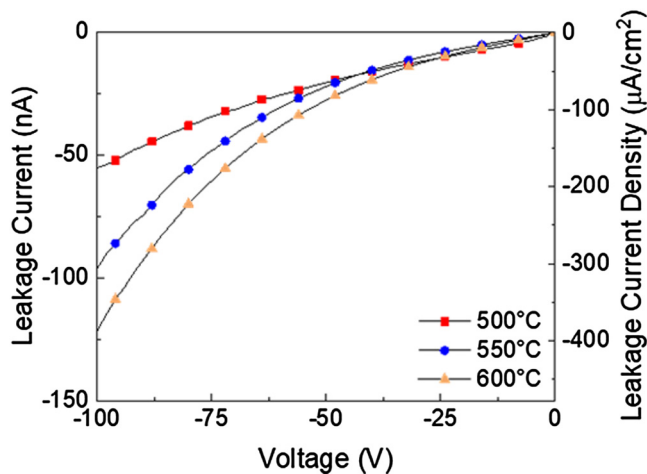


FIG. 3. Effect of annealing temperature on reverse bias voltage leakage current and current density for W/Au rectifiers annealed at 500 , 550 , and $600\text{ }^{\circ}\text{C}$ for 3 min.

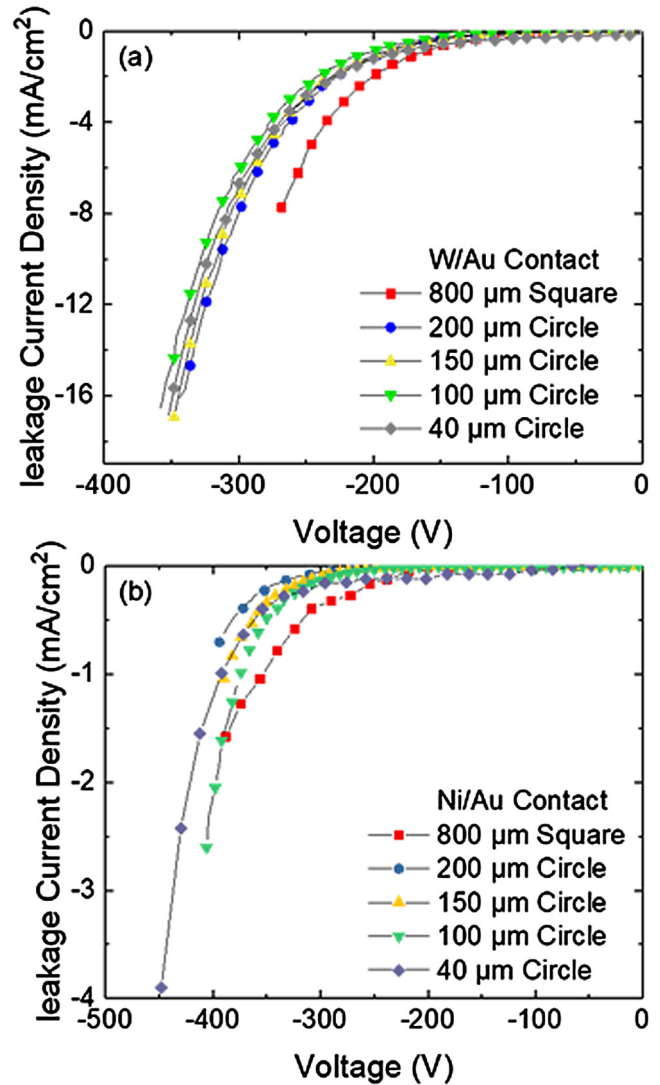


FIG. 4. Reverse leakage current density characteristics for W/Au Schottky contacts of different size and shape annealed for 5 min at $500\text{ }^{\circ}\text{C}$ (a) and for Ni/Au contacts of a similar geometry as deposited (b).

geometry contact device shows lower current density relative to the circular devices. We have noted that these square geometry structures are more resistant to degradation during voltage stressing, due to anisotropic heating properties of Ga₂O₃. Similar data are shown in Fig. 4 (bottom) for Ni/Au, with high breakdown voltages ~ 450 V. For this doping, the theoretical maximum breakdown voltage is ~ 4000 V and our experimental values correspond to maximum electric field strengths of $\sim 1.05\text{ MV cm}^{-1}$. Current state of the art rectifier structures contain stacking faults with a density of $1.5 \times 10^{10}\text{ cm}^{-2}$, threading screw dislocation densities of 30 cm^{-2} , and basal dislocation densities of 20 cm^{-2} .^{43–45} The presence of these defects is known to reduce the breakdown voltage. Note that the doping in the drift region was not affected by annealing, as shown in the C^{-2} -V data of Fig. 5, which shows that the drift region carrier concentration was unchanged at $3.53 \times 10^{16}\text{ cm}^{-3}$ for as-deposited and $500\text{ }^{\circ}\text{C}$, 300 s annealed W/Au samples. By comparison, the Ni/Au samples showed a similar value of $3.23 \times 10^{16}\text{ cm}^{-3}$.

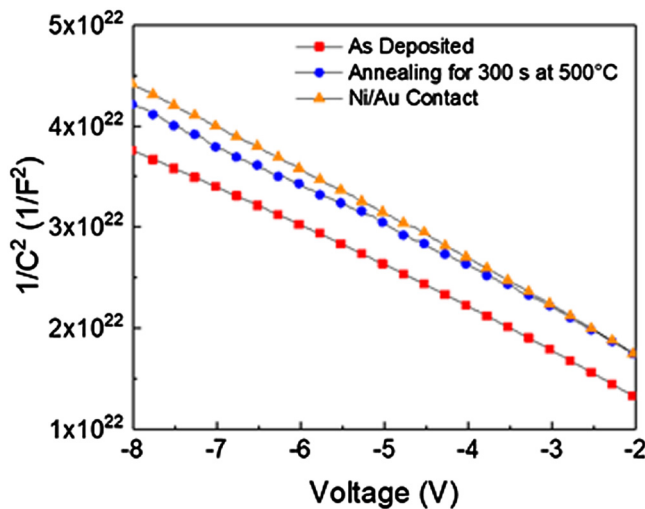


FIG. 5. C^{-2} - V characteristics of Ni/Au and W/Au contact as deposited and W/Au contact annealed for 5 min at 500 °C.

This rules out a change in the drift layer concentration as a result of the increased current with annealing.

The surface morphology of the W/Au contacts showed little change with annealing time at 500 °C. Examples are shown in the AFM scans of Fig. 6, with the root mean square roughness measured over a $10 \times 10 \mu\text{m}^2$ area being 4.2 nm for the as-deposited contact and 6.6 nm after annealing at 500 °C for 300 s. This is consistent with the AES scans shown in Fig. 7, where there is no measurable change in the slope of the Au and W profiles at that interface or of

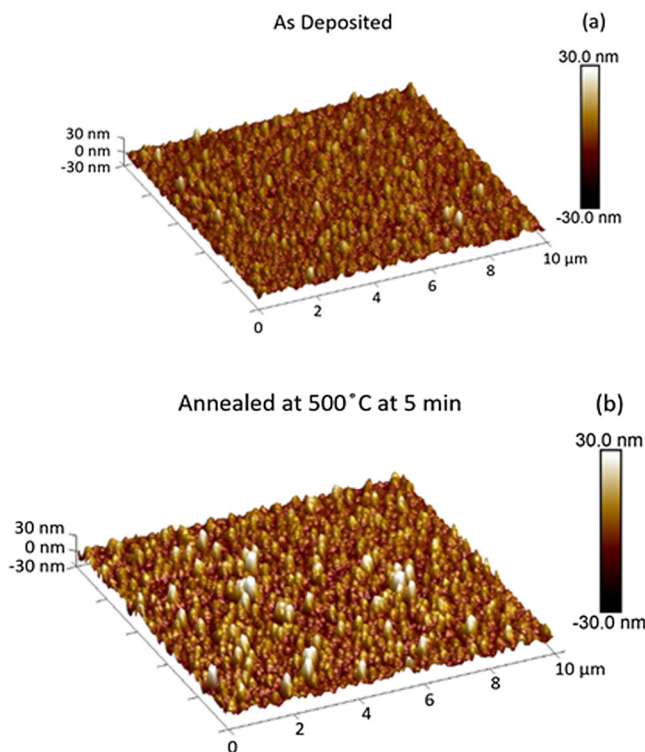


FIG. 6. Atomic force microscope images of W/Au contact as deposited (a) and (b) annealed at 500 °C for 5 min.

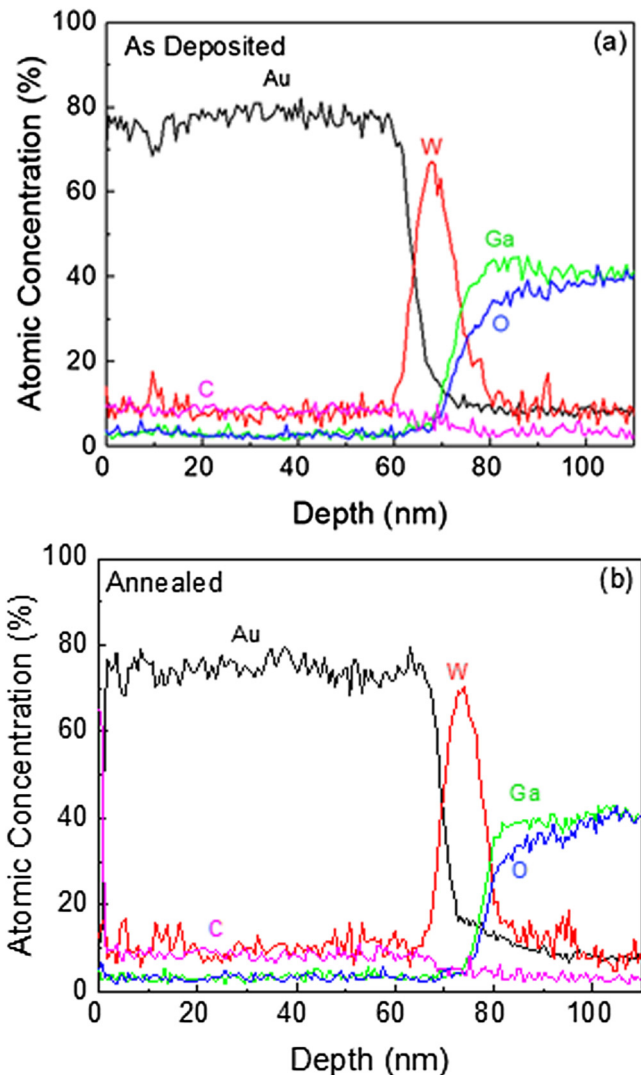


FIG. 7. Auger electron analysis depth profile for W/Au contact as deposited (a) and (b) annealed at 500 °C for 5 min.

the W/Ga₂O₃ interface after annealing at 500 °C for 300 s. This indicates no significant reaction of either Au with W or the latter with the underlying Ga₂O₃. This is to be contrasted with the clear degradation of Ni contacts at the same annealing temperature reported previously.³²

The high current switching behavior of the rectifiers is of interest. Figure 8(a) shows the schematic of the circuit used to examine the switching behavior from high forward currents to large reverse voltages. The design of this circuit has been reported in detail previously.^{46–48} In short, it consists of an inductor (J.W. Miller 1140–153K-RC, 15 mH), the Ga₂O₃ rectifiers under test, and a power transistor (STMicroelectronics STW9N150, 1.5 kV, 8 A n-channel MOSFET) controlled by a pulse signal. A Ga₂O₃ Schottky diode has a minimal current overshoot during the switch from forward-biased conduction to the reverse blocking state because the reverse recovery time only depends on the capacitance, rather than on the minority carrier recombination. At startup, the inductor is charged from the DC power supply to accumulate energy by turning on the power

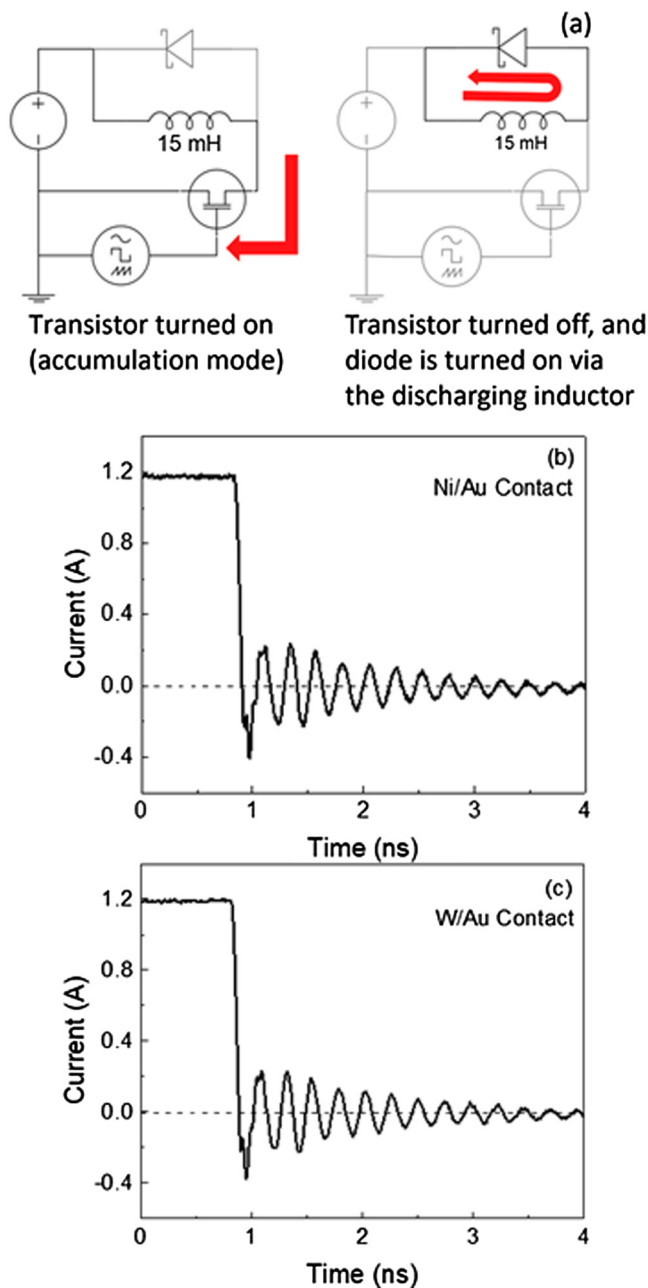


FIG. 8. Schematic of switching test circuit (a) showing that the inductor is being charged by the DC power supply (left) and discharges to turn on the Schottky diode (right). Diode switching characteristics from 1.2 A forward current (b) to reverse bias of -300 V for Ni/Au diode and (c) W/Au contact annealed for 5 min at 500 °C for a fixed rectifier area of $600 \times 600 \mu\text{m}^2$.

switching transistor. When the power transistor turns off, the inductor current is discharged through the forward-biased rectifier.

Experimental switching performance from the W/Au and Ni/Au rectifiers is shown in Figs. 8(b) and 8(c), respectively, for switching 1.2 A forward current to -300 V reverse bias. The reverse recovery times were the same for both types of contacts (99 ns for Ni/Au and 100 ns for W/Au) and dI/dt values of 2.14 A/ μS for Ni/Au and 2.23 A/ μS for W/Au. This shows that W is well-suited to handling large current loads during switching.

IV. SUMMARY AND CONCLUSIONS

The electrical performance of (001) β -Ga₂O₃ vertical diodes with W/Au Schottky contacts was studied at various annealing times and the temperature range from 500 to 600 °C. The barrier height after removal of sputter damage is 0.81 eV, lower than for the standard Ni/Au (1.07 eV), but the former is more thermally stable and remains an option for high temperature applications. The barrier heights on (001) orientation are lower than on (-201) , which shows a value of 0.97 eV. The W/Au contacts show an onset of increased reverse leakage current for anneals at ≥ 550 °C, but have on/off ratios $>10^6$ over a broad bias range. They show excellent switching characteristic from high forward currents to a reverse bias of -300 V.

ACKNOWLEDGMENTS

The project was sponsored by the Department of the Defense, Defense Threat Reduction Agency (No. HDTRA1-17-1-011), monitored by Jacob Calkins and also by NSF DMR (No. 1856662, Tania Paskova). Research at NRL was supported by the Office of Naval Research, partially under Award No. N00014-15-1-2392. The content of the information does not necessarily reflect the position or the policy of the federal government, and no official endorsement should be inferred. The authors at NCTU would like to thank the Ministry of Science and Technology, Taiwan, for the financial support under Grant Nos. MOST 107-2918-I-009-010 and 108-2636-E-009-008.

¹H. von Wenckstern, *Adv. Electron. Mater.* **3**, 1600350 (2017).

²M. Higashiwaki and G. H. Jessen, *Appl. Phys. Lett.* **112**, 060401 (2018).

³S. J. Pearton, J. Yang, P. H. Cary, F. Ren, J. Kim, M. J. Tadjer, and M. A. Mastro, *Appl. Phys. Rev.* **5**, 011301 (2018).

⁴Z. Galazka, *Semicond. Sci. Technol.* **33**, 113001 (2018).

⁵S. Rafique, L. Han, A. T. Neal, S. Mou, M. J. Tadjer, R. H. French, and H. Zhao, *Appl. Phys. Lett.* **109**, 132103 (2016).

⁶K. Konishi, K. Goto, H. Murakami, Y. Kumagai, A. Kuramata, S. Yamakoshi, and M. Higashiwaki, *Appl. Phys. Lett.* **110**, 103506 (2017).

⁷K. Zeng and U. Singiseti, *Appl. Phys. Lett.* **111**, 122108 (2017).

⁸S. J. Pearton, Fan Ren, Marko Tadjer, and Jihyun Kim, *J. Appl. Phys.* **124**, 222901 (2018).

⁹W. Li, Z. Hu, K. Nomoto, R. Jinno, Z. Zhang, T. Q. Tu, K. Sasaki, A. Kuramata, D. Jena, and G. H. Xing, *2018 IEEE International Electron Devices Meeting (IEDM)*, San Francisco, CA, 1–5 December 2018 (IEEE, New York, 2018), p. 8.5.1.

¹⁰B. K. Bose, *Proc. IEEE* **105**, 2007 (2017).

¹¹Woongkul Lee, Di Han Silong Li, Bulent Sarlioglu, Tatiana A. Minav, and Matti Pietola, *IEEE Trans. Transport. Electrification* **4**, 684 (2018).

¹²R. J. Kaplar, A. A. Allerman, A. M. Armstrong, M. H. Crawford, J. R. Dickerson, A. J. Fischer, A. G. Baca, and E. A. Douglas, *ECS J. Solid State Sci. Technol.* **6**, Q3061 (2017).

¹³M. A. Mastro, A. Kuramata, J. Calkins, J. Kim, F. Ren, and S. J. Pearton, *ECS J. Solid State Sci. Technol.* **6**, 356 (2017).

¹⁴Q. He et al., *IEEE Electron Device Lett.* **39**, 556 (2018).

¹⁵J. Bae, H. W. Kim, I. H. Kang, G. Yang, and J. Kim, *Appl. Phys. Lett.* **112**, 122102 (2018).

¹⁶S. B. Reese, T. Remo, J. Green, and A. Zakutayev, *Joule* **3**, 903 (2019).

¹⁷Marko Tadjer, *Electrochem. Soc. Interface* **27**, 49 (2018).

¹⁸Z. Hu et al., *Appl. Phys. Lett.* **113**, 122103 (2018).

¹⁹Chia-Hung Lin, et al., "Vertical Ga₂O₃ Schottky Barrier Diodes with Guard Ring Formed by Nitrogen-Ion Implantation," *Proceedings of the 2019 Compound Semiconductor Week (CSW)*, Nara, Japan, 19–23 May 2019 (IEEE, New York, 2019).

- ²⁰J. C. Yang, F. Ren, M. J. Tadjer, S. J. Pearton, and A. Kuramata, *ECS J. Solid State Sci. Technol.* **7**, Q92 (2018).
- ²¹J. C. Yang, F. Ren, M. J. Tadjer, S. J. Pearton, and A. Kuramata, *IEEE Trans. Electron Devices* **65**, 2790 (2018).
- ²²J. C. Yang, F. Ren, Marko Tadjer, S. J. Pearton, and A. Kuramata, *AIP Adv.* **8**, 055026 (2018).
- ²³Jiancheng Yang *et al.*, *Appl. Phys. Lett.* **114**, 232106 (2019).
- ²⁴Patrick H. Carey IV, Jiancheng Yang, Fan Ren, Ribhu Sharma, Mark Law, and Stephen J. Pearton, *ECS J. Solid State Sci. Technol.* **8**, Q3221 (2019).
- ²⁵T. J. Anderson *et al.*, *ECS J. Solid State Sci. Technol.* **6**, Q3036 (2017).
- ²⁶M. Mohamed, K. Imscher, C. Janowitz, Z. Galazka, R. Manzke, and R. Fornari, *Appl. Phys. Lett.* **101**, 132106 (2012).
- ²⁷M. H. Wong, Y. Nakata, A. Kuramata, S. Yamakoshi, and M. Higashiwaki, *Appl. Phys. Express* **10**, 041101 (2017).
- ²⁸Y. Yao, R. F. Davis, and L. M. Porter, *J. Electron. Mater.* **46**, 2053 (2017).
- ²⁹Q. He *et al.*, *Appl. Phys. Lett.* **110**, 093503 (2017).
- ³⁰Y. Yao, R. Gangireddy, J. Kim, K. K. Das, R. F. Davis, and L. M. Porter, *J. Vac. Sci. Technol. B* **35**, 03D113 (2017).
- ³¹Luke A. M. Lyle, Lai Jiang, Kalyan K. Das, and Lisa M. Porter, "Gallium oxide technology, devices and applications," in *Schottky Contacts to Ga₂O₃*, edited by S. Pearton, F. Ren, and M. Mastro (Elsevier, London, 2019).
- ³²Chaker Fares, Fan Ren, and S. J. Pearton, *ECS J. Solid State Sci. Technol.* **8**, Q3007 (2019).
- ³³J. E. N. Swallow, J. B. Varley, L. A. H. Jones, J. T. Gibbon, L. F. J. Piper, V. R. Dhanak, and T. D. Veal, *APL Mater.* **7**, 022528 (2019).
- ³⁴Marko Tadjer, "Ohmic contacts to gallium oxide, in gallium oxide technology," in *Devices and Applications*, edited by S. Pearton, F. Ren, and M. Mastro (Elsevier, London, 2019).
- ³⁵E. H. Rhoderick, *IEEE Proc. I Solid State Electron Devices* **129**, 1 (1982).
- ³⁶Fan Ren, J. C. Yang, Chaker Fares, and S. J. Pearton, *MRS Commun.* **9**, 77 (2019).
- ³⁷E. Farzana, Z. Zhang, P. Paul, A. R. Arehart, and S. A. Ringel, *Appl. Phys. Lett.* **110**, 202102 (2017).
- ³⁸A. Fiedler, R. Schewski, Z. Galazka, and K. Imscher, *ECS J. Solid State Sci. Technol.* **8**, Q3083 (2019).
- ³⁹M. Higashiwaki *et al.*, *Appl. Phys. Lett.* **108**, 133503 (2016).
- ⁴⁰Shihyun Ahn, F. Ren, L. Yuan, S. J. Pearton, and A. Kuramata, *ECS J. Solid State Sci. Technol.* **6**, 68 (2017).
- ⁴¹Z. Zhang, E. Farzana, A. Arehart, and S. Ringel, *Appl. Phys. Lett.* **108**, 052105 (2016).
- ⁴²S. Oh, G. Yang, and J. Kim, *ECS J. Solid State Sci. Technol.* **6**, Q3022 (2017).
- ⁴³T. Oishi, Y. Koga, K. Harada, and M. Kasu, *Appl. Phys. Express* **8**, 031101 (2015).
- ⁴⁴T. Oishi, K. Harada, Y. Koga, and M. Kasu, *Jpn. J. Appl. Phys.* **55**, 030305 (2016).
- ⁴⁵Nadeemullah A. Mahadik, Marko J. Tadjer, Peter L. Bonanno, Karl D. Hobart, Robert E. Stahlbush, Travis J. Anderson, and Akito Kuramata, *APL Mater.* **7**, 022513 (2019).
- ⁴⁶Yen-Ting Chen, J. C. Yang, Fan Ren, Chin-Wei Chang, Jenshan Lin, S. J. Pearton, Marko J. Tadjer, Akito Kuramata, and Yu-Te Liao, *ECS J. Solid State Sci. Technol.* **8**, Q3229 (2019).
- ⁴⁷J. Yang, F. Ren, Y. Chen, Y. Liao, C. Chang, J. Lin, M. Tadjer, S. J. Pearton, and A. Kuramata, *IEEE J. Electron Devices Soc.* **7**, 57 (2019).
- ⁴⁸J. C. Yang *et al.*, *ECS J. Solid State Sci. Technol.* **8**, Q3028 (2019).